

# SceneMaker: Open-set 3D Scene Generation with Decoupled De-occlusion and Pose Estimation Model

Yukai Shi<sup>1,3\*</sup> Weiyu Li<sup>2,4</sup> Zihao Wang<sup>4</sup> Hongyang Li<sup>3</sup> Xingyu Chen<sup>3</sup> Ping Tan<sup>2,4</sup> Lei Zhang<sup>3</sup>  
<sup>1</sup> Tsinghua University <sup>2</sup> HKUST <sup>3</sup> IDEA Research <sup>4</sup> LightIllusions



Figure 1. Our method not only achieves superior performance in both **indoor** and **open-set** scenarios but also demonstrates stronger generalization across **synthetic** and **real-world captured** images.

## Abstract

We propose a decoupled 3D scene generation framework called **SceneMaker** in this work. Due to the lack of sufficient open-set de-occlusion and pose estimation priors, existing methods struggle to simultaneously produce high-quality geometry and accurate poses under severe occlusion and open-set settings. To address these issues, we first decouple the de-occlusion model from 3D object generation, and enhance it by leveraging image datasets and collected

de-occlusion datasets for much more diverse open-set occlusion patterns. Then, we propose a unified pose estimation model that integrates global and local mechanisms for both self-attention and cross-attention to improve accuracy. Besides, we construct an open-set 3D scene dataset to further extend the generalization of the pose estimation model. Comprehensive experiments demonstrate the superiority of our decoupled framework on both indoor and open-set scenes. Our codes and datasets is released at <https://idea-research.github.io/SceneMaker/>.

\*Done during internship at IDEA Research.

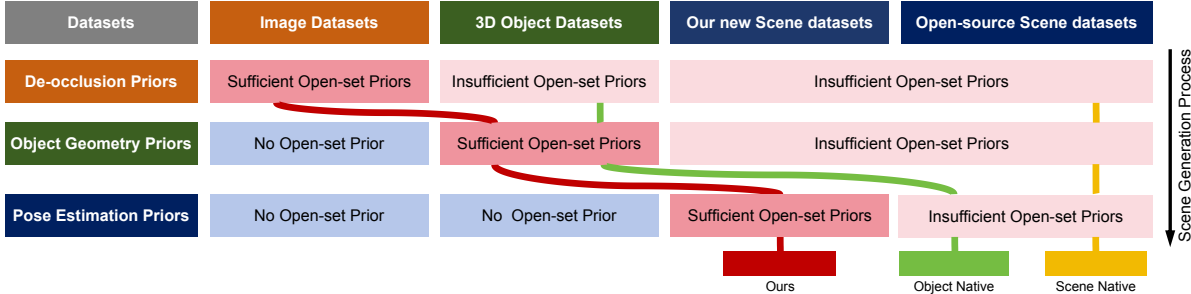


Figure 2. **The analysis of prior sources in different methods.** The table shows that the availability of required open-set priors (column) varies across different datasets (row). Paths in different colors represent various scene generation methods. Existing methods (**yellow path** and **green path**) lack sufficient open-set priors for de-occlusion and pose estimation due to the limited datasets. We further leverage image datasets for de-occlusion and collect new scene datasets for pose estimation to achieve better open-set performance(**red path**).

## 1. Introduction

Open-set 3D scene generation aims to synthesize 3D scenes containing arbitrary objects in any open-world domain from a single image. It is a fundamental task with high demand in AIGC and embodied AI, including applications such as 3D asset creation, simulation environment construction, and 3D perception for decision-making. However, limited scene datasets [4, 13, 18] have confined most existing methods [7, 11, 12, 14, 19, 31, 34, 45] to constrained domains like indoor scenes.

Recently, the advent of large-scale 3D object datasets [15] has driven rapid progress in open-set 3D object generation models [26–28, 52, 54, 58, 60], and emerging methods [3, 22, 29, 33, 55] are beginning to extend scene generation toward open-set settings. Despite all the progress, existing methods still struggle to simultaneously produce high-quality geometry and accurate poses under severe occlusion and open-set settings in Figure 10.

The root cause is the model’s insufficient open-set priors for de-occlusion and pose estimation. As illustrated in Figure 2, a 3D scene generation model requires three key open-set priors in columns: de-occlusion, object geometry, and pose estimation. The availability of these priors varies across scene, object, and image datasets in rows [4, 15, 16, 18, 41]. Paths in different colors represent various scene generation methods with different prior sources. Existing scene-native methods (**yellow path**) [12, 14, 31, 45] attempt to learn all the three priors exclusively from scene datasets, where the availability of open-set priors is limited. Object-native methods (**green path**) [3, 22, 29, 33, 38, 53, 55] further leverage large-scale 3D object datasets to learn sufficient open-set object geometry priors. However, the open-set priors for de-occlusion and pose estimation still remain insufficient due to the limited datasets, leaving these challenges unresolved. Meanwhile, existing pose estimation methods [51, 56, 57] suffer from performance degradation in scene generation task, primarily due to missing size prediction and the absence of tailored attention mechanisms for different pose variables.

In this paper, we further advance 3D scene generation towards open-set scenarios by addressing the critical issue of insufficient de-occlusion and pose estimation priors, as shown in Figure 2 (**red path**). Specifically, we construct a decoupled framework that divides 3D scene generation into three distinct tasks based on the necessary priors: de-occlusion, 3D object generation, and pose estimation. Each task is trained separately on image datasets, 3D object datasets, and scene datasets, respectively. The decoupled framework ensures that each task can maximize the learning of its corresponding open-set priors, preventing quality degradation caused by the cross-impact of data on tasks, such as geometry collapse of small objects and pose shifting resulting from the joint representation of geometry and pose as shown in Figure. 10.

Second, we develop a robust de-occlusion model by leveraging image datasets for open-set occlusion prior. Image datasets are significantly larger than 3D datasets, encompassing a broader range of open-set objects and exhibiting more diverse occlusion patterns. To maintain the sufficient open-set priors, we adopt the image editing model [25] as the initialization. Then, we finetune it on our 10K image de-occlusion dataset with three carefully designed occlusion patterns to further enhance its de-occlusion capability, resulting in the final de-occlusion model. Compared with existing 3D object-based methods [22, 53], our model achieves higher quality and more text-controllable results under severe occlusion and open-set conditions.

Third, we propose a unified pose estimation model along with a 200K scene dataset for better performance and open-set generalization. Since 3D object generation models [6, 26, 58, 60] usually output normalized objects in canonical space for better geometry, existing methods [5, 51, 56, 57] often restrict to predefined classes or miss size prediction when they are employed in scene generation task. Thus, we propose a unified diffusion-based pose estimation model, which directly predicts object rotation, translation, and size conditioned on point clouds, images, and object geometry. Compared to existing methods [55], we introduce both sin-

gle object and multi-object self-attention mechanism to ensure interactions between objects for coherent relationships. Moreover, we design a decoupled cross-attention mechanism, where rotation attends to canonical object conditions, while translation and scale attend to scene-level conditions, to further improve accuracy. Additionally, to extend open-set capability, we construct a large-scale synthetic dataset of 200K scenes using Objaverse [15] objects and mix it with existing scene datasets during training.

Finally, comprehensive experiments demonstrate that our model achieves state-of-the-art performance in both object geometry quality and pose accuracy on both indoor and open-set test sets. We further discuss the method’s generalization to varying numbers of objects and its potential upper bound under video and multi-view modalities.

In summary, our contributions are as threefold:

- We construct a decoupled 3D scene generation framework called **SceneMaker** that fully exploits existing datasets to learn sufficient open-set priors for de-occlusion and pose estimation, achieving superior performance in comprehensive experiments.
- We develop a robust de-occlusion model by leveraging image datasets for open-set occlusion priors and enhancing it with our 10K object image de-occlusion dataset.
- We propose a unified pose estimation diffusion model that directly predicts each object’s 6D pose and size, introducing both local and global attention mechanisms to enhance accuracy. And we further curate a 200K synthesized scene dataset for open-set generalization.

## 2. Related Work

### 2.1. 3D Scene Generation

3D scene generation is in high demand for AIGC and embodied AI, serving as a foundation task for real-to-sim applications. Based on the source of 3D objects, existing methods fall into two categories: generation-based and retrieval-based. Retrieval-based methods [14] retrieve 3D objects from offline libraries but struggle to generalize to open-set scenarios due to limited asset diversity. Generation-based methods directly generate 3D objects from images and can be categorized into scene-native and object-native methods. Scene-native methods [12, 31, 45] directly learn from scene datasets [4, 13, 18] but are limited to specific domains like indoor scenes. Object-native methods further leverage open-set 3D object datasets [15] to improve object geometry quality. A series of methods [3, 22, 29, 33, 55] directly generate object geometry in the scene space. However, due to the limitations of scene datasets and the coupled representation, they often suffer from obvious degradation on images with severe occlusion or small objects. Another series of methods [55] decouple geometry generation and pose estimation to improve

the open-set performance. But they lack scene-level interactions during pose estimation, leading to inaccurate relative poses. Fundamentally, existing methods lack sufficient de-occlusion and pose estimation priors. We supplement both open-set priors by leveraging image datasets for de-occlusion and proposing a unified model along with synthetic scene datasets for pose estimation.

### 2.2. Object Generation under Occlusion

With the emergence of large-scale open-set 3D object datasets [15], a number of native 3D object generation works [26, 28, 52, 54, 58, 60] have achieved impressive results. However, generating 3D objects under occlusion conditions is more aligned with the needs of scene generation and still requires further exploration. Most existing methods [9, 10, 43, 62] model the task as 3D completion, where partial geometry is derived from images and subsequently completed using 3D generation models. Recently, some methods [8, 53] additionally use occluded images and masks as supplementary information to achieve better performance. Since 3D generation models already possess sufficient geometric priors, the bottleneck is the lack of de-occlusion priors. Image datasets, which contain more diverse occlusion patterns than 3D datasets, have not been fully utilized. We address this by decoupling the de-occlusion model and leveraging image datasets for training to enhance quality and controllability.

### 2.3. Pose Estimation

Model-based pose estimation aims to predict poses based on the given CAD model. Existing methods [46, 47, 59, 61] have achieved impressive performance on predefined classes. Recent works [24, 42, 51, 56, 57] further extend the task to arbitrary objects with regression or diffusion models. However, they lack the size prediction when they are employed on scene generation task. CAST3D [55] address the issue with a point diffusion model, but it lacks both interaction between objects and decoupled mechanism with conditions from different spaces. We propose a unified pose estimation diffusion model with both local and global attention mechanisms to improve accuracy.

## 3. Method

In this work, we construct a decoupled 3D scene generation framework called **SceneMaker** that fully exploits existing datasets to learn sufficient open-set priors. In Section 3.1, we formulate and overview the whole scene generation framework. In Section 3.2 we introduce how to leverage image datasets for decoupled de-occlusion model in 3D object generation. In Section 3.3, we propose the unified pose estimation model and extend open-set generalization with synthetic datasets.

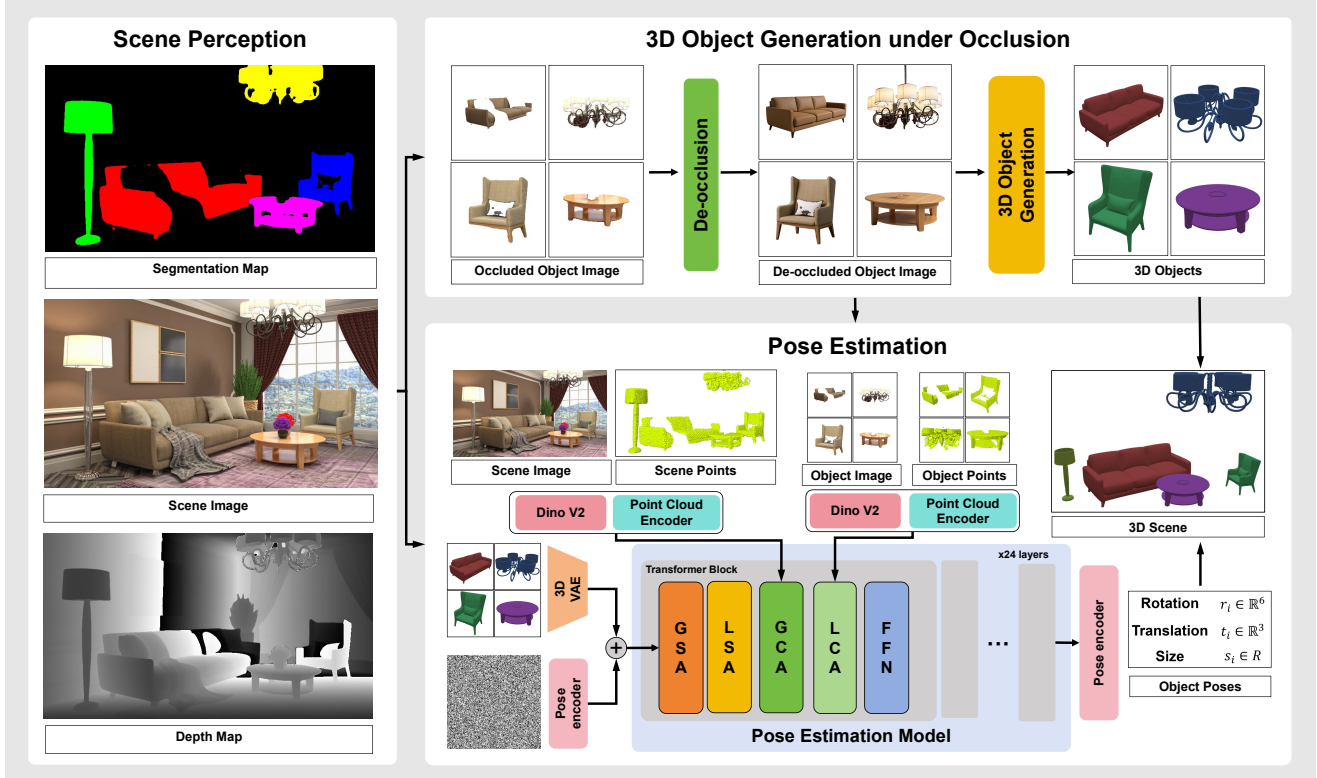


Figure 3. **The Framework of SceneMaker.** Our framework consists of scene perception, 3D object generation under occlusion, and pose estimation. We decouple the de-occlusion model from 3D object generation. We construct a unified pose estimation model that incorporates both global and local attention mechanisms. GSA, LSA, GCA, LCA, and FFN denote global self-attention, local self-attention, global cross-attention, local cross-attention, and feed-forward network, respectively.

### 3.1. Framework

As shown in Figure 3, given a single scene image  $X$  containing multiple objects  $X = \{x_1, x_2, \dots, x_n\}$ , our scene generation framework aims to generate a consistent 3D scene  $Z$  containing corresponding 3D objects  $Z = \{z_1, z_2, \dots, z_n\}$ . Our framework consists of three modules: scene perception, 3D object generation under occlusion, and pose estimation, which are formally following the subsequent automated steps.

- Utilize Grounded-SAM [40] to segment object masks  $M = \{m_1, m_2, \dots, m_n\}$ . Apply the mask on the scene image  $X$  to obtain occluded object images  $I = \{i_1, i_2, \dots, i_n\}$ .
- Utilize MoGe [49] to estimate scene depth map  $D$ . Apply mask  $M$  on the depth and project pixels into 3D space to obtain point clouds  $C = \{c_1, c_2, \dots, c_n\}$ .
- Acquire de-occluded object images  $I^d = \{i_1^d, i_2^d, \dots, i_n^d\}$  with  $\epsilon_\theta^d(I_t^d; t, I) \rightarrow I^d$ , where  $\epsilon_\theta^d$  denotes our decoupled de-occlusion model and  $t$  denotes timesteps in diffusion models.
- Generate 3D object geometry  $O = \{o_1, o_2, \dots, o_n\}$  based on de-occluded images  $I^d$  with  $\epsilon_\theta^o(O_t; t, I^d) \rightarrow O$ , where  $\epsilon_\theta^o$  denotes the 3D generation model.

- Estimate object poses  $P = \{p_1, p_2, \dots, p_n\}$  based on point clouds, images and object geometry with  $\epsilon_\theta^p(P_t; t, X, M, I, C, O) \rightarrow P$ , where  $\epsilon_\theta^p$  denotes the pose estimation model. Here the object poses contain rotation, translation, and size:  $p_i = \{r_i, t_i, s_i\}$ .
- Composite generated object geometry and estimated poses into the final scene:  $Z = \{O, P\}$ .

In this formulation, we construct the decoupled 3D scene generation framework that fully exploits existing datasets to learn sufficient open-set priors.

### 3.2. Object Generation with De-occlusion Model

After obtaining the depth map and segmentation masks from the scene perception module, we aim to generate 3D objects with the high-quality geometry based on occluded object images. However, existing methods often struggle to generate high-quality geometry under severe occlusion. The main challenge is that models lack sufficient open-set occlusion priors due to limited 3D datasets.

Image datasets are significantly larger than 3D datasets, encompassing a broader range of open-set objects and more diverse occlusion patterns. Therefore, compared with existing methods, we further decoupled the de-occlusion model

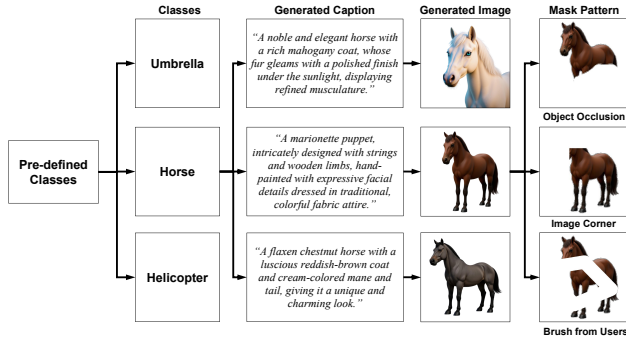


Figure 4. The curation pipeline of de-occlusion datasets.

and train it on image datasets for richer occlusion priors. The de-occlusion model is formulated as follow:

$$\epsilon_{\theta}^d(I_t^d; t, I) \rightarrow I^d, \quad (1)$$

where  $\epsilon_{\theta}^d$ ,  $I$ ,  $I^d$ ,  $t$  denote our decoupled de-occlusion model, occluded images, de-occluded images, and timesteps in diffusion models, respectively.

Since existing 3D native object generation models [26, 54, 58, 60] have achieved impressive performance, we simply adopt existing methods [27] for image-3d generation after de-occlusion, as shown in Equation 2:

$$\epsilon_{\theta}^o(O_t; t, I^d) \rightarrow O, \quad (2)$$

where  $\epsilon_{\theta}^o$  and  $O$  denote the 3D generation model and generated 3D objects, respectively.

### 3.2.1. De-occlusion Model

We finetune Flux Kontext [25] on our de-occlusion datasets to obtain the de-occlusion model. To acquire sufficient open-set priors and a strong understanding of natural language prompts, we directly employ Flux Kontext [25] as the initialization for our de-occlusion model. Although both editing [25] and inpainting [23] models can achieve de-occlusion, their performance is often suboptimal in cases of severe occlusion. The fundamental cause is the lack of diverse and severe occlusion patterns in the training data. To address this issue, we construct an additional 10K object image de-occlusion dataset for finetuning to further enhance its de-occlusion capability.

**De-occlusion Datasets.** The curation pipeline is shown in Figure 4. We first use GPT [2] to generate detailed captions of objects, and then employ an image generation model [17] to produce high-quality target images. Considering that occluded images are derived from the segmentation model [40] based on predefined class labels [32], we generate 20 captions per class, and further expand them as detailed as possible to ensure high-quality images. Meanwhile, we create a universal template as the de-occlusion text prompt for all classes. Next, we carefully design three masking strategies to simulate real-world occlusions: object cutouts without background for object occlusion, right-angle cropping for image borders, and random brush strokes



Figure 5. The occlusion patterns of de-occlusion datasets.

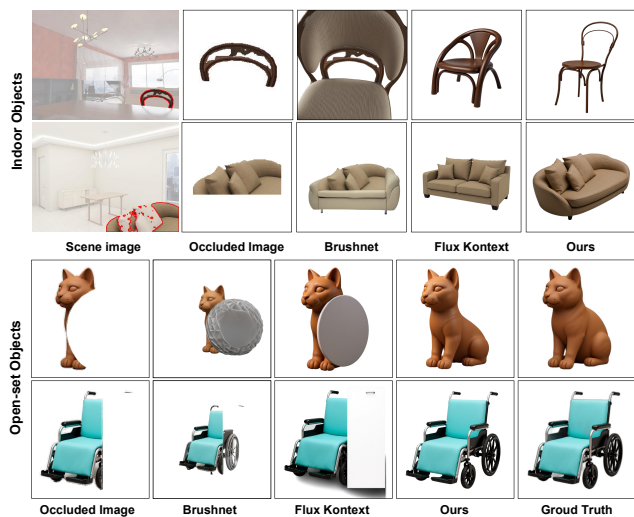


Figure 6. Qualitative comparison of de-occlusion models. Our model has better performance on both indoor and open-set objects, especially under severe occlusion.

Methods	PSNR $\uparrow$	SSIM $\uparrow$	CLIP $\uparrow$
BrushNet [23]	11.07	0.6760	0.2659
Flux Kontext [25]	13.91	0.7309	0.2674
Ours	<b>15.03</b>	<b>0.7566</b>	<b>0.2698</b>

Table 1. Quantitative comparison of de-occlusion.

for user prompts, as shown in Figure 5. We also random resize the object and the whole image to simulate patterns of small objects and low-resolution images. Finally, the de-occlusion dataset is constructed by 10K triplets formed by masked images, text prompts, and target images.

### 3.2.2. Comparison

**De-occlusion.** We conduct both quantitative and qualitative experiments to demonstrate the superiority of our de-occlusion model. We mainly compare our model with the state-of-the-art methods in image painting [23] and image editing [25]. We evaluate these methods on our collected validation set of 1K images spanning over 500 classes. We use PSNR and SSIM between the prediction and ground

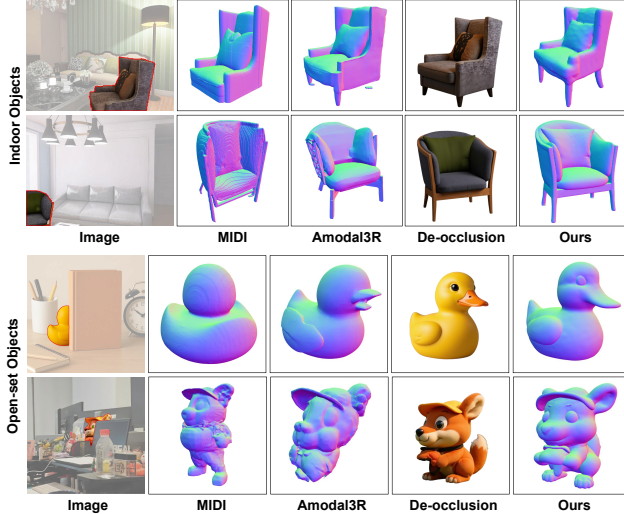


Figure 7. Qualitative comparison of object generation under occlusion. Our model has more complete and detailed geometry on both indoor and open-set objects.

Methods	CD ↓	F-Score ↑	Volume IoU ↑
MIDI [22]	0.0508	0.5533	0.4214
Amodal3R [53]	0.0443	0.7124	0.5279
Ours	<b>0.0409</b>	<b>0.7454</b>	<b>0.5985</b>

Table 2. Quantitative comparison of object generation under occlusion. Our decoupled method achieves better performance.

truth images, as well as the CLIP score [39] between the prediction image and class labels, as evaluation metrics. As shown in Figure 6 and Table 1, our de-occlusion model achieve better performance on both indoor and open-set scenes, especially under severe occlusions.

**Object Generation under Occlusion.** To demonstrate the superiority of our decoupled pipeline, we compare it with both existing 3D native object generation methods [53] and scene generation methods [22] on the occluded 3D object generation task. As shown in Table 2, to align with real-world occlusion patterns, we use images rendered from the 3D-Front dataset [18] by InstPifu [31] as the test set in our quantitative experiments, which contains numerous objects of severe occlusion. We further conduct qualitative experiments on indoor and open-set scenes in Figure 7. Both qualitative and quantitative results show that our decoupled framework achieves superior performance in occluded object generation across both indoor and open-set scenes.

### 3.3. Unified Pose Estimation Model

The goal of the pose estimation model is to predict each object’s rotation  $R$ , translation  $T$ , and size  $S$  in the scene based on its canonical geometry  $O$ . Existing methods [22, 51, 55–57] mainly face three challenges. First, they often miss size prediction when they are employed in scene generation task, since object geometries are usually generated in canonical space. Second, they do not properly decouple

different pose variables when interacting with scene-level and object-level features, resulting in performance degradation. To address these two issues, we propose a unified pose estimation model that incorporates both global and local attention mechanisms in Section 3.3.1. Third, existing methods often struggle on open-set scenarios due to limited datasets. We build a large-scale open-set dataset containing over 200K synthesized scenes to tackle the generalization challenge in Section 3.3.2.

#### 3.3.1. Pipeline

As shown in Figure 3, we propose a unified pose estimation model that introduces both global and local attention mechanisms specific for the scene generation task. We directly incorporate object size into the prediction and jointly estimate it with rotation and translation, to address the adaptation challenge in scene generation task. Specifically, we take scene images  $X$ , scene masks  $M$ , cropped object images  $I$ , point clouds  $C$ , and object geometries  $O$  as inputs, and predict object rotation  $R$ , translation  $T$ , and size  $S$  as outputs, where rotation is represented in 6D.

To improve learning efficiency, all scenes are normalized to a unified space for pose estimation. Since all pose variables can be well represented within a Gaussian distribution, we employ the diffusion model [21, 30, 36] for pose estimation from a generative perspective, where poses are denoised from Gaussian noise with the input modalities serving as conditioning signals. The final formulation can be represented in Equation 3.

$$\begin{aligned} \epsilon_{\theta}^p(P_t; t, X, M, I, C, O) &\rightarrow P, \\ P &= \{R, T, S\}, \end{aligned} \quad (3)$$

where  $\epsilon_{\theta}^p$ ,  $t$  denote the pose estimation model and timestep in diffusion models, respectively.

As shown in Figure 3, the trainable object pose encoder and decoder are composed of MLPs. Object geometries, images, and point clouds are encoded into features using a pretrained 3D object VAE, Dinov2 [35], and a point encoder pretrained on 3D reconstruction tasks, all of which are kept frozen during training. Object geometry is injected through concatenation with pose tokens, while image and point cloud features are injected via cross-attention. We implement our model using a flow matching framework [30] with a DiT architecture [36], where each transformer block consists of global and local self-attention, global and local cross-attention, and a feed-forward network.

**Attention Mechanisms.** As shown in Figure 8, we adopt both global and local mechanisms for self-attention and cross-attention. Each pose variable is separately encoded as a token, so each object in the diffusion model is uniquely represented by a quadruple of tokens: rotation, translation, size, and geometry. The local self-attention module enables the interaction inside the quadruple of each object. The global self-attention module enables tokens of all objects

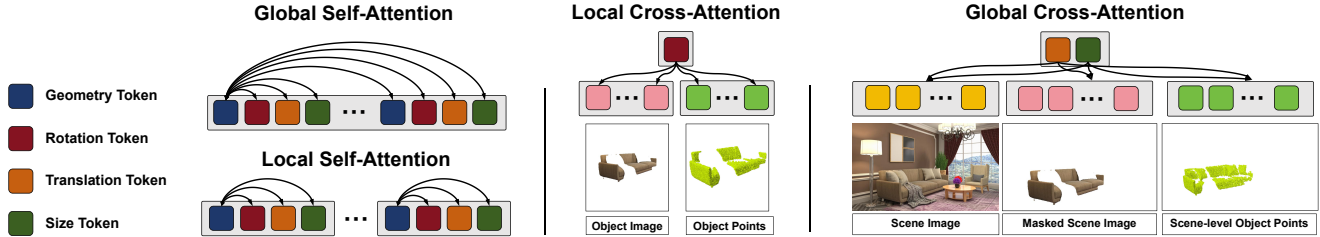


Figure 8. **Attention mechanisms in the pose estimation model.** The global self-attention module enables tokens of all objects in the scene to interact with each other. The local cross-attention module enables rotation tokens independently interact with conditions in the object canonical space. The global cross-attention module enables translation and size tokens attend to scene-level conditions.

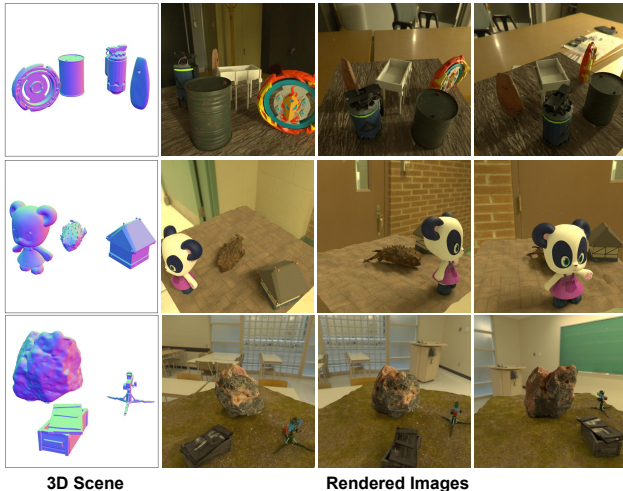


Figure 9. **The samples of collected open-set dataset.**

in the scene to interact with each other, leading to more coherent relative object poses. Considering that rotation can be independently estimated in the object canonical space and scene-level conditions provide little benefit, we introduce a local cross-attention module, allowing the rotation token to attend only to the cropped object image and normalized object point cloud. Meanwhile, we retain a global cross-attention module for the translation and size tokens, allowing them to attend to the scene-level point cloud and image. This fine-grained attention mechanism is demonstrated effective in our comprehensive experiments.

### 3.3.2. Open-set Scene Datasets

Since existing datasets currently lack the necessary prior for training a 3D scene generation model in an open-set domain, we addressed this by constructing our own training data. This involved using a carefully curated subset of the existing Objaverse [15] dataset along with Blender [1]. A significant number of models in Objaverse are either scanned data or have low-quality textures and materials, which necessitated a rigorous curation process. To filter the models, we assessed their material information, excluding any that were transparent, lacked a BSDF node, or did not have an albedo map. To further refine the selection, we also

excluded models with pure or excessively dark albedo colors. Ultimately, this process resulted in a high-quality subset of 90k models with a superior appearance to construct a dataset of 200k scenes for our work.

We composed each scene by combining 2 to 5 randomly selected objects. To enhance realism, we used random environment maps sampled from Polyhaven [37] to serve as the background of the scenes. Additionally, we added a ground plane with a high-quality texture beneath the objects, using Perlin noise to enhance the surface and add realistic variations. Finally, each object was given a random rotation to serve as an augmentation of the level of the object to train the pose estimation module.

Each scene is rendered using Blender’s CYCLES engine from 20 viewpoints in 512 resolution, with camera elevations randomly sampled between  $[15, 60]$  degrees. Simultaneously, we also uniformly sampled 20k random points on the object’s surface to serve as the input geometric information for our object generation module. We also augment the background of images with random selection. To ensure physical plausibility, we place the lowest point of each object on the same plane and enforce that their bounding boxes do not intersect. We present samples from our dataset in Figure 9. We randomize the pitch angle of input meshes during training to better align 3D object generation outputs. This entire process resulted in a dataset of 200k scenes, comprising a total of 8 million images.

### 3.3.3. Training

We directly apply L2 loss to rotation, translation, and size, with equal weighting for each term. To demonstrate the superiority of our framework, we first train our model only on the 3D Front datasets [18] for fair comparison. We mix the datasets curated by MIDI3D [22] and Instpifu [31]. We align their render results according to room IDs, resulting in 20K scenes. We take 1K scenes as test sets and the rest as training sets. We train the model from scratch for 25K steps. To extend the generalization on open-set, we further mix our 200K open-set datasets into the indoor datasets, and take 1K scenes as open-set test sets. We train the model from scratch for 40K steps until the model converged.

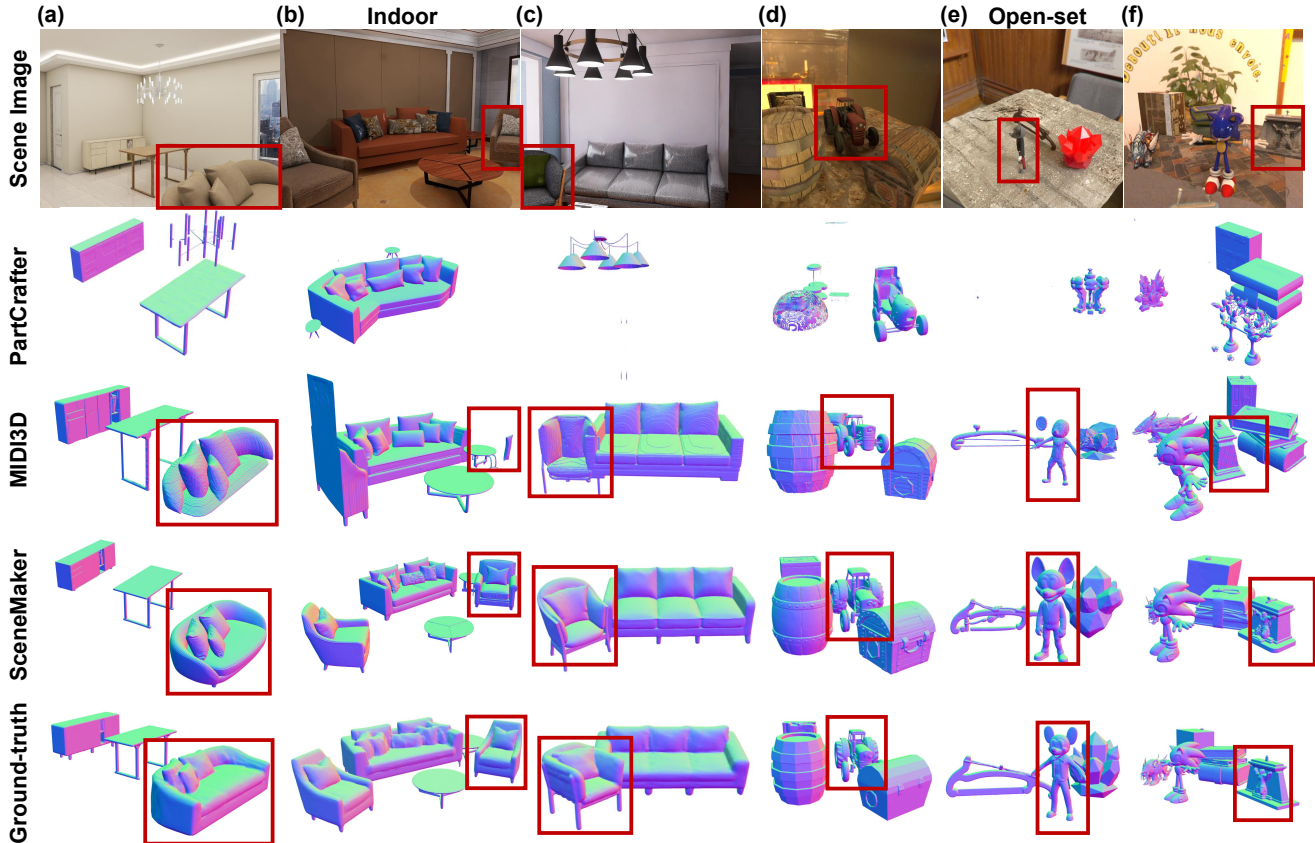


Figure 10. Qualitative comparison with scene generation methods.

Method	3D-Front					Open-set				
	CD-S↓	F-Score-S↑	CD-O↓	F-Score-O↑	IoU-B↑	CD-S↓	F-Score-S↑	CD-O↓	F-Score-O↑	IoU-B↑
PartCrafter [29]	0.1846	0.3844	-	-	-	0.2171	0.2613	-	-	-
MIDI3D [22]	0.1672	0.3420	0.0663	0.5495	0.3855	0.1425	0.3211	0.0807	0.5602	0.5079
SceneMaker (w/o open-set data)	<b>0.0381</b>	<b>0.6840</b>	<b>0.0681</b>	0.6160	0.7658	0.1538	0.4644	0.0847	0.5771	0.6248
SceneMaker(Ours)	0.0470	0.6312	0.0885	<b>0.6812</b>	<b>0.7693</b>	<b>0.0285</b>	<b>0.6125</b>	<b>0.0671</b>	<b>0.5948</b>	<b>0.7549</b>

Table 3. Quantitative comparison on indoor and open-set test sets with severe occlusions.

## 4. Experiments

### 4.1. Settings

**Datasets and Baselines.** We conduct experiments on both indoor and open-set datasets. Specifically, we conduct quantitative comparisons with existing methods [3, 7, 11, 19, 20, 22, 31, 34] on the MIDI [22] test set containing 1K scenes to demonstrate the superiority of our framework. To further validate the generalization of our method under severe occlusions and open-set scenarios, we randomly select 1K scenes with no overlap with the training set from 3D-front [18] as indoor test sets, and 1K scenes from our collected open-set data as open-set test sets. It is worth noting that our 3D-Front scenes contain significantly more occlusions compared to MIDI test set. We conduct both quantitative and qualitative comparison with SOTA meth-

ods MIDI [22] and PartCrafter [29]. We also conduct qualitative comparisons on synthetic, in-the-wild, and real-world captured images from a wider range of application domains.

**Metrics.** Following existing scene generation methods [22, 29, 55], we use scene-level Chamfer Distance (CD-S), F-Score (F-Score-S), and IoU Bounding Box (IoU-B) to evaluate the quality of the whole scene. And we use object-level Chamfer Distance (CD-O) and F-Score (F-Score-O) to evaluate the quality of generated object geometry.

### 4.2. Quantitative Results

As shown in Table 4, we conduct a quantitative evaluation on the MIDI test set with a wide range of existing methods [3, 7, 11, 19, 20, 22, 31, 34], and our approach achieves the best overall performance. As shown in Ta-

ble 3, our method consistently outperforms existing SOTA methods [22, 29], achieving the highest metrics on the more challenging indoor and open-set scene generation tasks. Remarkably, even without being trained on the open-set dataset, our method still obtains the best quantitative results on indoor scenes, which underscores the superiority of our proposed framework and designed modules.

Method	CD-S $\downarrow$	F-Score-S $\uparrow$	CD-O $\downarrow$	F-Score-O $\uparrow$	IoU-B $\uparrow$
PanoRecon [11]	0.150	0.4065	0.211	0.3505	0.240
Total3D [34]	0.270	0.3290	0.179	0.3638	0.238
InstPIFu [31]	0.138	0.3999	0.165	0.3811	0.299
SSR [7]	0.140	0.3976	0.170	0.3779	0.311
DiffCAD [19]	0.117	0.4358	0.190	0.3745	0.392
Gen3DSR [3]	0.123	0.4007	0.157	0.3811	0.363
REPARO [20]	0.129	0.4168	0.160	0.4085	0.339
MIDI [22]	0.080	0.5019	0.103	0.5358	0.518
SceneMaker	<b>0.051</b>	<b>0.5642</b>	<b>0.0963</b>	<b>0.6544</b>	<b>0.671</b>

Table 4. Quantitative comparison on MIDI test set [22].

### 4.3. Qualitative Results

As shown in Figure 10, our method generates visually compelling scenes that are not only realistic but also rich in detail. Crucially, our model demonstrates a robust ability to handle severe occlusions in Figure(a)(b), accurately reasoning about the relative spatial relationships between objects and places objects in plausible poses in Figure(c)(d)(f). Besides, our model can also handle small objects without geometry degradation in Figure(e).

We conduct more qualitative comparisons on both indoor and open-set scenes in Figure 13 and Figure 14, including both synthetic and real-world captured images. Our method offers better generalization to open-set scenes. Moreover, it delivers more accurate poses and finer geometry under severe occlusion or for small objects.

### 4.4. Ablation Study

**Attention Mechanism.** We ablate the contribution of the global and local self-attention mechanism, and the decoupled cross-attention mechanism in the pose estimation model respectively. For the self-attention mechanism, we simply remove the global and local attention modules respectively for comparison. For the decoupled cross-attention mechanism, we remove the local attention and merge the rotation update into the global attention for comparison. We train the above models from scratch and use ground-truth meshes to eliminate the influence of geometry on pose estimation. As shown in Table 5, all modules in our proposed attention mechanisms contribute positively to the performance, which underscores their superiority.

**Generalization on number of objects.** As shown in Figure 11, we conduct experiments scene images containing varying numbers of objects to demonstrate the model’s generalization capability. Although each scene in the training set contains no more than five objects, thanks to the de-

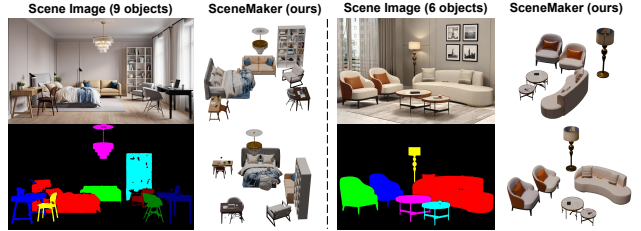


Figure 11. Ablation on the number of objects in the scene.

Method	CD-S $\downarrow$	FS-S $\uparrow$	CD-O $\downarrow$	FS-O $\uparrow$	IoU-B $\uparrow$
SceneMaker	<b>0.0242</b>	<b>0.7502</b>	<b>0.0294</b>	<b>0.8121</b>	<b>0.7555</b>
w/o GSA	0.0340	0.6610	0.0556	0.6293	0.7336
w/o LSA	0.0293	0.7434	0.0901	0.7142	0.7733
w/o LCA	0.0274	0.7368	0.0429	0.7113	<u>0.7882</u>
+ Complete points	<b>0.0064</b>	<b>0.9197</b>	<b>0.0124</b>	<b>0.8432</b>	<b>0.8550</b>

Table 5. Quantitative results of ablation studies. **Bold** and underline indicate the best and the second best, respectively.

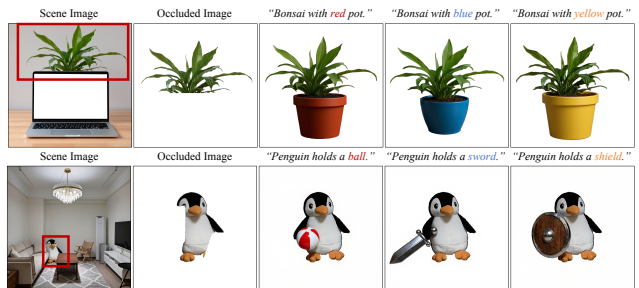


Figure 12. Text controllable object de-occlusion.

sign of RoPE [44], our pose estimation model generalizes well to scenes with more than five objects.

**Open-set Datasets.** We demonstrate the necessity of our proposed scene datasets on the open-set images as shown in Table 3. Our model faces severe degradation in open-set scenario without the datasets. The datasets mainly provide open-set patterns of diverse objects, which help build pose mappings across different geometries and are essential for open-set scene generation.

**Controllable object generation.** Benefiting from our decoupled de-occlusion model, compared with 3D native methods [22, 53], our model further enables controllable generation of the occluded areas of objects through prompts. As shown in Figure 12, our model is able to control the color of the pot and things in the penguin’s hand through prompts during de-occlusion.

**Upper Bound of Pose Estimation.** Compared to a single image, videos or multi-image can provide richer scene structure information through point cloud reconstruction. When the reconstruction algorithm [48, 50] reaches its upper limit, it is equivalent to providing our model with a complete point cloud. We discuss the upper bound of our pose estimation model by giving the complete point clouds. As shown in Table 5, with a complete point cloud, our model achieves a significant performance boost, demonstrating its strong potential under video or multi-image conditions.

## 5. Conclusion

In this paper, we propose a decoupled 3D scene generation framework called **SceneMaker**. To obtain sufficient occlusion priors, we decouple and develop the robust de-occlusion model from 3D object generation by leveraging image generation models and a 10K curated de-occlusion dataset for training. To improve the accuracy of the pose estimation model, we propose a unified pose estimation diffusion model with both local and global attention mechanisms. We further construct a 200K synthesized scene dataset for open-set generalization. Comprehensive experiments demonstrate the superiority of our framework on both indoor and open-set scenes.

**Limitations and future work.** Although our framework effectively generalizes to arbitrary objects, the real-world arrangement of objects is often much more complex than what our datasets capture, particularly when force interactions are involved. Therefore, a key future research topic is how to construct or refine 3D scenes more accurately in a physically plausible manner, including interpenetration and force interactions. Meanwhile, existing methods can only control scene generation through images or simple captions, and further development is needed for more control signals and natural language interactions. Moreover, how to perform more in-depth understanding tasks and adapt embodied decision-making based on generated high-quality 3D scenes is also an unsolved challenge.

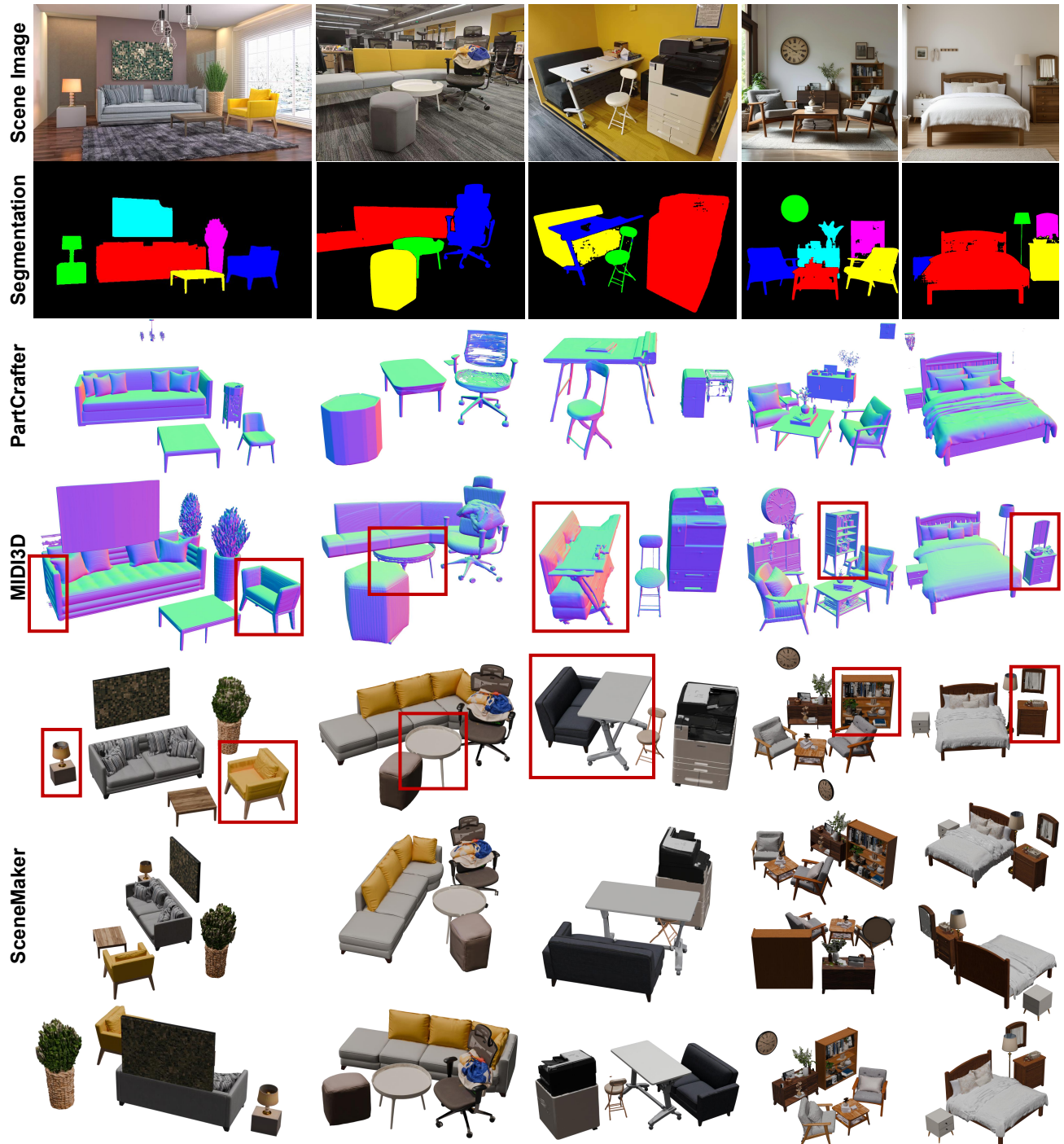


Figure 13. Qualitative comparison with scene generation methods on indoor scenes.

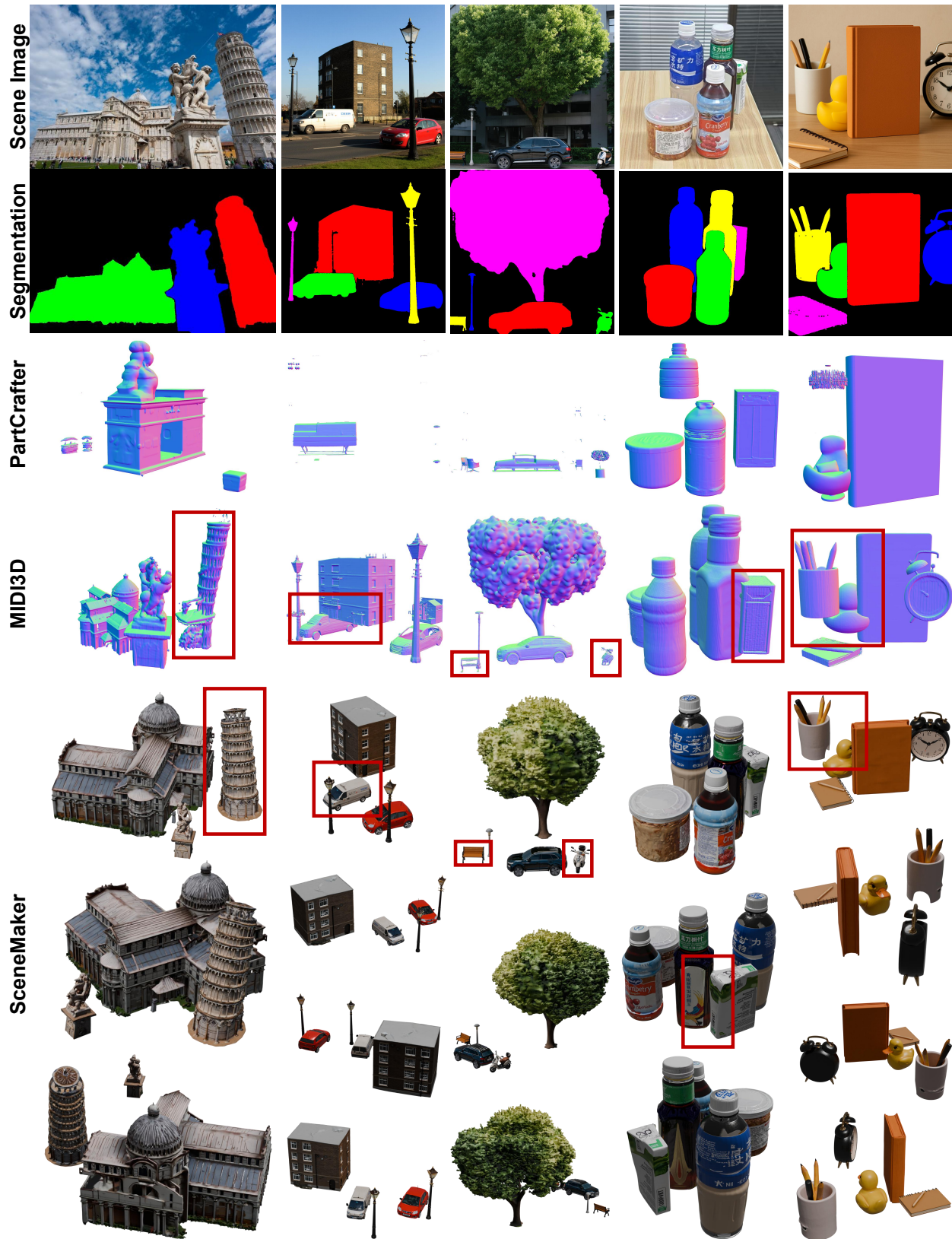


Figure 14. Qualitative comparison with scene generation methods on open-set scenes.

## References

- [1] Blender, 2025. <https://www.blender.org/>. 7
- [2] Josh Achiam, Steven Adler, Sandhini Agarwal, Lama Ahmad, Ilge Akkaya, Florencia Leoni Aleman, Diogo Almeida, Janko Altenschmidt, Sam Altman, Shyamal Anadkat, et al. Gpt-4 technical report. *arXiv preprint arXiv:2303.08774*, 2023. 5
- [3] Andreea Ardelean, Mert Özer, and Bernhard Egger. Gen3dsr: Generalizable 3d scene reconstruction via divide and conquer from a single view. *arXiv preprint arXiv:2404.03421*, 2024. 2, 3, 8, 9
- [4] Dejan Azinović, Ricardo Martin-Brualla, Dan B Goldman, Matthias Nießner, and Justus Thies. Neural rgb-d surface reconstruction. In *Proceedings of the IEEE/CVF Conference on Computer Vision and Pattern Recognition*, pages 6290–6301, 2022. 2, 3
- [5] Garrick Brazil, Abhinav Kumar, Julian Straub, Nikhila Ravi, Justin Johnson, and Georgia Gkioxari. Omni3d: A large benchmark and model for 3d object detection in the wild. In *Proceedings of the IEEE/CVF conference on computer vision and pattern recognition*, pages 13154–13164, 2023. 2
- [6] Rui Chen, Jianfeng Zhang, Yixun Liang, Guan Luo, Weiyu Li, Jiarui Liu, Xiu Li, Xiaoxiao Long, Jiashi Feng, and Ping Tan. Dora: Sampling and benchmarking for 3d shape variational auto-encoders. In *Proceedings of the Computer Vision and Pattern Recognition Conference (CVPR)*, pages 16251–16261, 2025. 2
- [7] Yixin Chen, Junfeng Ni, Nan Jiang, Yaowei Zhang, Yixin Zhu, and Siyuan Huang. Single-view 3d scene reconstruction with high-fidelity shape and texture. In *2024 International Conference on 3D Vision (3DV)*, pages 1456–1467. IEEE, 2024. 2, 8, 9
- [8] Junhyeong Cho, Kim Youwang, Hunmin Yang, and Tae-Hyun Oh. Robust 3d shape reconstruction in zero-shot from a single image in the wild. In *Proceedings of the Computer Vision and Pattern Recognition Conference*, pages 22786–22798, 2025. 3
- [9] Ruihang Chu, Enze Xie, Shentong Mo, Zhenguo Li, Matthias Nießner, Chi-Wing Fu, and Jiaya Jia. Diffcomplete: Diffusion-based generative 3d shape completion. *Advances in neural information processing systems*, 36:75951–75966, 2023. 3
- [10] Ruikai Cui, Weizhe Liu, Weixuan Sun, Senbo Wang, Taizhang Shang, Yang Li, Xibin Song, Han Yan, Zhennan Wu, Shenzhou Chen, et al. Neusdfusion: A spatial-aware generative model for 3d shape completion, reconstruction, and generation. In *European Conference on Computer Vision*, pages 1–18. Springer, 2024. 3
- [11] Manuel Dahnert, Ji Hou, Matthias Nießner, and Angela Dai. Panoptic 3d scene reconstruction from a single rgb image. *Advances in Neural Information Processing Systems*, 34: 8282–8293, 2021. 2, 8, 9
- [12] Manuel Dahnert, Angela Dai, Norman Müller, Angela, and Matthias Nießner. Coherent 3d scene diffusion from a single rgb image. In *Thirty-Eighth Conference on Neural Information Processing Systems*, 2024. 2, 3
- [13] Angela Dai, Angel X Chang, Manolis Savva, Maciej Halber, Thomas Funkhouser, and Matthias Nießner. Scannet: Richly-annotated 3d reconstructions of indoor scenes. In *Proceedings of the IEEE conference on computer vision and pattern recognition*, pages 5828–5839, 2017. 2, 3
- [14] Tianyuan Dai, Josiah Wong, Yunfan Jiang, Chen Wang, Cem Gokmen, Ruohan Zhang, Jiajun Wu, and Li Fei-Fei. Automated creation of digital cousins for robust policy learning. *arXiv preprint arXiv:2410.07408*, 2024. 2, 3
- [15] Matt Deitke, Dustin Schwenk, Jordi Salvador, Luca Weihs, Oscar Michel, Eli VanderBilt, Ludwig Schmidt, Kiana Ehsani, Aniruddha Kembhavi, and Ali Farhadi. Objaverse: A universe of annotated 3d objects. In *Proceedings of the IEEE/CVF conference on computer vision and pattern recognition*, pages 13142–13153, 2023. 2, 3, 7
- [16] Jia Deng, Wei Dong, Richard Socher, Li-Jia Li, Kai Li, and Li Fei-Fei. Imagenet: A large-scale hierarchical image database. In *2009 IEEE conference on computer vision and pattern recognition*, pages 248–255. Ieee, 2009. 2
- [17] Flux. Flux [Text-to-Image Model]. <https://blackforestlabs.ai/announcing-black-forest-labs/>, 2024. 5
- [18] Huan Fu, Bowen Cai, Lin Gao, Ling-Xiao Zhang, Jiaming Wang, Cao Li, Qixun Zeng, Chengyue Sun, Rongfei Jia, Binqiang Zhao, et al. 3d-front: 3d furnished rooms with layouts and semantics. In *Proceedings of the IEEE/CVF International Conference on Computer Vision*, pages 10933–10942, 2021. 2, 3, 6, 7, 8
- [19] Daoyi Gao, Dávid Rozenberszki, Stefan Leutenegger, and Angela Dai. Diffcad: Weakly-supervised probabilistic cad model retrieval and alignment from an rgb image. *ACM Transactions on Graphics (TOG)*, 43(4):1–15, 2024. 2, 8, 9
- [20] Haonan Han, Rui Yang, Huan Liao, Jiankai Xing, Zunnan Xu, Xiaoming Yu, Junwei Zha, Xiu Li, and Wanhua Li. Reparo: Compositional 3d assets generation with differentiable 3d layout alignment. In *Proceedings of the IEEE/CVF International Conference on Computer Vision*, pages 25367–25377, 2025. 8, 9
- [21] Jonathan Ho, Ajay Jain, and Pieter Abbeel. Denoising diffusion probabilistic models. *Advances in neural information processing systems*, 33:6840–6851, 2020. 6
- [22] Zehuan Huang, Yuan-Chen Guo, Xingqiao An, Yunhan Yang, Yangguang Li, Zi-Xin Zou, Ding Liang, Xihui Liu, Yan-Pei Cao, and Lu Sheng. Midi: Multi-instance diffusion for single image to 3d scene generation. *arXiv preprint arXiv:2412.03558*, 2024. 2, 3, 6, 7, 8, 9
- [23] Xuan Ju, Xian Liu, Xintao Wang, Yuxuan Bian, Ying Shan, and Qiang Xu. Brushnet: A plug-and-play image inpainting model with decomposed dual-branch diffusion. In *European Conference on Computer Vision*, pages 150–168. Springer, 2024. 5
- [24] Yann Labbé, Lucas Manuelli, Arsalan Mousavian, Stephen Tyree, Stan Birchfield, Jonathan Tremblay, Justin Carpentier, Mathieu Aubry, Dieter Fox, and Josef Sivic. Megapose: 6d pose estimation of novel objects via render & compare. *arXiv preprint arXiv:2212.06870*, 2022. 3

- [25] Black Forest Labs, Stephen Batifol, Andreas Blattmann, Frederic Boesel, Saksham Consul, Cyril Diagne, Tim Dockhorn, Jack English, Zion English, Patrick Esser, et al. Flux. 1 kontext: Flow matching for in-context image generation and editing in latent space. *arXiv preprint arXiv:2506.15742*, 2025. 2, 5
- [26] Weiyu Li, Jiarui Liu, Rui Chen, Yixun Liang, Xuelin Chen, Ping Tan, and Xiaoxiao Long. Craftsman: High-fidelity mesh generation with 3d native generation and interactive geometry refiner. *arXiv preprint arXiv:2405.14979*, 2024. 2, 3, 5
- [27] Weiyu Li, Xuanyang Zhang, Zheng Sun, Di Qi, Hao Li, Wei Cheng, Weiwei Cai, Shihao Wu, Jiarui Liu, Zihao Wang, et al. Step1x-3d: Towards high-fidelity and controllable generation of textured 3d assets. *arXiv preprint arXiv:2505.07747*, 2025. 5
- [28] Yangguang Li, Zi-Xin Zou, Zexiang Liu, Dehu Wang, Yuan Liang, Zhipeng Yu, Xingchao Liu, Yuan-Chen Guo, Ding Liang, Wanli Ouyang, et al. Triposg: High-fidelity 3d shape synthesis using large-scale rectified flow models. *arXiv preprint arXiv:2502.06608*, 2025. 2, 3
- [29] Yuchen Lin, Chenguo Lin, Panwang Pan, Honglei Yan, Yiqiang Feng, Yadong Mu, and Katerina Fragkiadaki. Partcrafter: Structured 3d mesh generation via compositional latent diffusion transformers. *arXiv preprint arXiv:2506.05573*, 2025. 2, 3, 8, 9
- [30] Yaron Lipman, Ricky TQ Chen, Heli Ben-Hamu, Maximilian Nickel, and Matt Le. Flow matching for generative modeling. *arXiv preprint arXiv:2210.02747*, 2022. 6
- [31] Haolin Liu, Yujian Zheng, Guanying Chen, Shuguang Cui, and Xiaoguang Han. Towards high-fidelity single-view holistic reconstruction of indoor scenes. In *European Conference on Computer Vision*, pages 429–446. Springer, 2022. 2, 3, 6, 7, 8, 9
- [32] Shilong Liu, Zhaoyang Zeng, Tianhe Ren, Feng Li, Hao Zhang, Jie Yang, Qing Jiang, Chunyuan Li, Jianwei Yang, Hang Su, et al. Grounding dino: Marrying dino with grounded pre-training for open-set object detection. In *European conference on computer vision*, pages 38–55. Springer, 2024. 5
- [33] Yanxu Meng, Haoning Wu, Ya Zhang, and Weidi Xie. SceneGen: Single-image 3d scene generation in one feedforward pass. *arXiv preprint arXiv:2508.15769*, 2025. 2, 3
- [34] Yinyu Nie, Xiaoguang Han, Shihui Guo, Yujian Zheng, Jian Chang, and Jian Jun Zhang. Total3dunderstanding: Joint layout, object pose and mesh reconstruction for indoor scenes from a single image. In *Proceedings of the IEEE/CVF Conference on Computer Vision and Pattern Recognition*, pages 55–64, 2020. 2, 8, 9
- [35] Maxime Oquab, Timothée Darcet, Théo Moutakanni, Huy Vo, Marc Szafranec, Vasil Khalidov, Pierre Fernandez, Daniel Haziza, Francisco Massa, Alaaeldin El-Nouby, et al. Dinov2: Learning robust visual features without supervision. *arXiv preprint arXiv:2304.07193*, 2023. 6
- [36] William Peebles and Saining Xie. Scalable diffusion models with transformers. In *Proceedings of the IEEE/CVF International Conference on Computer Vision*, pages 4195–4205, 2023. 6
- [37] Poly Haven. Poly Haven. <https://polyhaven.com/>, 2025. 7
- [38] Yansong Qu, Shaohui Dai, Xinyang Li, Yuze Wang, You Shen, Liujuan Cao, and Rongrong Ji. Deocc-1-to-3: 3d de-occlusion from a single image via self-supervised multi-view diffusion. *arXiv preprint arXiv:2506.21544*, 2025. 2
- [39] Alec Radford, Jong Wook Kim, Chris Hallacy, Aditya Ramesh, Gabriel Goh, Sandhini Agarwal, Girish Sastry, Amanda Askell, Pamela Mishkin, Jack Clark, et al. Learning transferable visual models from natural language supervision. In *International conference on machine learning*, pages 8748–8763. PMLR, 2021. 6
- [40] Tianhe Ren, Shilong Liu, Ailing Zeng, Jing Lin, Kunchang Li, He Cao, Jiayu Chen, Xinyu Huang, Yukang Chen, Feng Yan, et al. Grounded sam: Assembling open-world models for diverse visual tasks. *arXiv preprint arXiv:2401.14159*, 2024. 4, 5
- [41] Christoph Schuhmann, Romain Beaumont, Richard Vencu, Cade Gordon, Ross Wightman, Mehdi Cherti, Theo Coombes, Aarush Katta, Clayton Mullis, Mitchell Wortsman, et al. Laion-5b: An open large-scale dataset for training next generation image-text models. *NeurIPS*, 2022. 2
- [42] Ivan Shugurov, Fu Li, Benjamin Busam, and Slobodan Ilic. Osop: A multi-stage one shot object pose estimation framework. In *Proceedings of the IEEE/CVF Conference on Computer Vision and Pattern Recognition*, pages 6835–6844, 2022. 3
- [43] David Stutz and Andreas Geiger. Learning 3d shape completion from laser scan data with weak supervision. In *Proceedings of the IEEE conference on computer vision and pattern recognition*, pages 1955–1964, 2018. 3
- [44] Jianlin Su, Murtadha Ahmed, Yu Lu, Shengfeng Pan, Wen Bo, and Yunfeng Liu. Roformer: Enhanced transformer with rotary position embedding. *Neurocomputing*, 568:127063, 2024. 9
- [45] Jiapeng Tang, Yinyu Nie, Lev Markhasin, Angela Dai, Justus Thies, and Matthias Nießner. Diffuscene: Denoising diffusion models for generative indoor scene synthesis. In *Proceedings of the IEEE/CVF conference on computer vision and pattern recognition*, pages 20507–20518, 2024. 2, 3
- [46] Meng Tian, Marcelo H Ang Jr, and Gim Hee Lee. Shape prior deformation for categorical 6d object pose and size estimation. In *European Conference on Computer Vision*, pages 530–546. Springer, 2020. 3
- [47] He Wang, Srinath Sridhar, Jingwei Huang, Julien Valentin, Shuran Song, and Leonidas J Guibas. Normalized object coordinate space for category-level 6d object pose and size estimation. In *Proceedings of the IEEE/CVF conference on computer vision and pattern recognition*, pages 2642–2651, 2019. 3
- [48] Jianyuan Wang, Minghao Chen, Nikita Karaev, Andrea Vedaldi, Christian Rupprecht, and David Novotny. Vggt: Visual geometry grounded transformer. *arXiv preprint arXiv:2503.11651*, 2025. 9
- [49] Ruicheng Wang, Sicheng Xu, Cassie Dai, Jianfeng Xiang, Yu Deng, Xin Tong, and Jiaolong Yang. Moge: Unlocking accurate monocular geometry estimation for open-domain

- images with optimal training supervision. In *Proceedings of the Computer Vision and Pattern Recognition Conference*, pages 5261–5271, 2025. 4
- [50] Shuzhe Wang, Vincent Leroy, Yohann Cabon, Boris Chidlovskii, and Jerome Revaud. Dust3r: Geometric 3d vision made easy. In *Proceedings of the IEEE/CVF Conference on Computer Vision and Pattern Recognition*, pages 20697–20709, 2024. 9
- [51] Bowen Wen, Wei Yang, Jan Kautz, and Stan Birchfield. Foundationpose: Unified 6d pose estimation and tracking of novel objects. In *Proceedings of the IEEE/CVF Conference on Computer Vision and Pattern Recognition*, pages 17868–17879, 2024. 2, 3, 6
- [52] Shuang Wu, Youtian Lin, Feihu Zhang, Yifei Zeng, Jingxi Xu, Philip Torr, Xun Cao, and Yao Yao. Direct3d: Scalable image-to-3d generation via 3d latent diffusion transformer. *arXiv preprint arXiv:2405.14832*, 2024. 2, 3
- [53] Tianhao Wu, Chuanxia Zheng, Frank Guan, Andrea Vedaldi, and Tat-Jen Cham. Amodal3r: Amodal 3d reconstruction from occluded 2d images. *arXiv preprint arXiv:2503.13439*, 2025. 2, 3, 6, 9
- [54] Jianfeng Xiang, Zelong Lv, Sicheng Xu, Yu Deng, Ruicheng Wang, Bowen Zhang, Dong Chen, Xin Tong, and Jiaolong Yang. Structured 3d latents for scalable and versatile 3d generation. In *Proceedings of the Computer Vision and Pattern Recognition Conference*, pages 21469–21480, 2025. 2, 3, 5
- [55] Kaixin Yao, Longwen Zhang, Xinhao Yan, Yan Zeng, Qixuan Zhang, Lan Xu, Wei Yang, Jiayuan Gu, and Jingyi Yu. Cast: Component-aligned 3d scene reconstruction from an rgb image. *arXiv preprint arXiv:2502.12894*, 2025. 2, 3, 6, 8
- [56] Jiyao Zhang, Mingdong Wu, and Hao Dong. Genpose: Generative category-level object pose estimation via diffusion models. *arXiv preprint arXiv:2306.10531*, 2023. 2, 3
- [57] Jiyao Zhang, Weiyao Huang, Bo Peng, Mingdong Wu, Fei Hu, Zijian Chen, Bo Zhao, and Hao Dong. Omni6dpose: A benchmark and model for universal 6d object pose estimation and tracking. In *European Conference on Computer Vision*, pages 199–216. Springer, 2024. 2, 3, 6
- [58] Longwen Zhang, Ziyu Wang, Qixuan Zhang, Qiwei Qiu, Anqi Pang, Haoran Jiang, Wei Yang, Lan Xu, and Jingyi Yu. Clay: A controllable large-scale generative model for creating high-quality 3d assets. *ACM Transactions on Graphics (TOG)*, 43(4):1–20, 2024. 2, 3, 5
- [59] Ruida Zhang, Yan Di, Fabian Manhardt, Federico Tombari, and Xiangyang Ji. Ssp-pose: Symmetry-aware shape prior deformation for direct category-level object pose estimation. In *2022 IEEE/RSJ International Conference on Intelligent Robots and Systems (IROS)*, pages 7452–7459. IEEE, 2022. 3
- [60] Zibo Zhao, Zeqiang Lai, Qingxiang Lin, Yunfei Zhao, Haolin Liu, Shuhui Yang, Yifei Feng, Mingxin Yang, Sheng Zhang, Xianghui Yang, et al. Hunyuan3d 2.0: Scaling diffusion models for high resolution textured 3d assets generation. *arXiv preprint arXiv:2501.12202*, 2025. 2, 3, 5
- [61] Linfang Zheng, Chen Wang, Yinghan Sun, Esha Dasgupta, Hua Chen, Aleš Leonardis, Wei Zhang, and Hyung Jin Chang. Hs-pose: Hybrid scope feature extraction for category-level object pose estimation. In *Proceedings of the IEEE/CVF conference on computer vision and pattern recognition*, pages 17163–17173, 2023. 3
- [62] Linqi Zhou, Yilun Du, and Jiajun Wu. 3d shape generation and completion through point-voxel diffusion. In *Proceedings of the IEEE/CVF international conference on computer vision*, pages 5826–5835, 2021. 3